https://doi.org/10.5194/bg-2020-167
Preprint. Discussion started: 8 June 2020


Biogeosciences Discussions
Open Access
EGU

# The suspended small-particles layer in the suboxic Black Sea: a proxy for delineating the effective $N_2$-yielding section

Rafael Rasse[1], Hervé Claustre[1], and Antoine Poteau[1]

[1]Sorbonne Université and CNRS, Laboratoire d'Océanographie de Villefranche (LOV) UMR7093, Institut de la Mer de Villefranche (IMEV), 06230, Villefranche-sur-Mer, France.

*Correspondence to*: rafael.rasse@obs-vlfr.fr; rjrasse@gmail.com

**Abstract.** Upper suboxic water masses confine a majority of the microbial communities that can produce up to 90% of oceanic $N_2$. This effective $N_2$-yielding section encloses a suspended small-particle layer, inferred from particle backscattering ($b_{bp}$) measurements. It is thus hypothesized that this layer (hereafter, the *$b_{bp}$-layer*) is linked to $N_2$-yielding microbial communities such as anammox and denitrifying bacteria — a hypothesis yet to be evaluated. Here, data collected by three BGC-Argo floats deployed in the Black Sea are used to investigate the origin of this *$b_{bp}$-layer*. To this end, we evaluate how key drivers of anammox-denitrifying bacteria dynamics impact on the vertical distribution of $b_{bp}$ and the thickness of the *$b_{bp}$-layer*. In conjunction with published data on $N_2$ excess, our results suggest that the *$b_{bp}$-layer* is at least partially composed of anammox-denitrifying bacteria for three main reasons: (1) strong correlations are recorded between $b_{bp}$ and nitrate; (2) the top location of the *$b_{bp}$-layer* is driven by the ventilation of oxygen-rich subsurface waters, while its thickness is modulated by the amount of nitrate available to produce $N_2$; (3) the maxima of both $b_{bp}$ and $N_2$ excess coincide at the same isopycnals where denitrifying-anammox bacteria coexist. We thus advance that $b_{bp}$ and $O_2$ can be exploited as a combined proxy to delineate the $N_2$-yielding section of the Black Sea. This proxy can potentially contribute to refining delineation of the effective $N_2$-yielding section of oxygen-deficient zones via data from the growing BGC-Argo float network.

## 1 Introduction

Suboxic water masses ($O_2 \leq 5$ µM) host denitrifying and anammox bacteria that produce between 20-40% of oceanic $N_2$, respectively via heterotrophic denitrification and anaerobic oxidation of ammonium (Gruber and Sarmiento, 1997; Ward 2013). The upper suboxic water masses of oceanic oxygen-deficient zones (ODZs) make up the most effective $N_2$-producing section because this is where the bacteria that condition the process mainly develop (Ward et al., 2009; Dalsgaard et al., 2012). For example, in such water masses in the open eastern tropical north Pacific, denitrifying and anammox bacteria can generate up to 90% of the $N_2$ lost in the ODZ core (Babin et al., 2014). It is thus important to unravel the biogeochemical parameters that trigger the accumulation of such bacteria in upper suboxic ODZs. This information is crucial for understanding and quantifying how bacterial biomass and related $N_2$ loss can respond to the ongoing expansion of ODZs (Keeling and Garcia, 2002; Stramma et al., 2008; Helm et al., 2011; Schmidtko et al., 2017). Ultimately, greater accuracy in this domain can contribute to improving mechanistic predictions on how such expansion affects the oceans' role in driving the Earth's climate by sequestering atmospheric carbon dioxide (e.g. Oschlies et al., 2018).

In suboxic water masses, the biogeochemical factors that can affect the abundance of denitrifying and anammox bacteria are the levels of $O_2$, organic matter (OM), nitrate ($NO_3^-$), ammonium ($NH_4^+$), and hydrogen sulfide ($H_2S$) (Murray et al., 1995; Ward et al., 2008; Dalsgaard et al., 2014; Bristow et al., 2016). Therefore, to elucidate what triggers the confinement of such

https://doi.org/10.5194/bg-2020-167
Preprint. Discussion started: 8 June 2020




bacteria, we need to investigate how the above biogeochemical factors drive their vertical distribution, with high temporal and vertical resolution. To this end, we should develop multidisciplinary approaches that allow us to permanently monitor the full range of biogeochemical variables of interest in suboxic ODZs.

Optical proxies of tiny particles can be applied as an alternative approach to assess the vertical distribution of $N_2$-yielding microbial communities in upper suboxic ODZs (Naqvi et al., 1993). For instance, anammox and denitrifying bacteria are found as free-living bacteria (0.2-2 µm), and can be associated with small-suspended (> 2-30 µm), and large-sinking (> 30 µm) particles (Fuchsman et al., 2012a, 2017; Ganesh et al., 2014, 2015). Therefore, particle backscattering ($b_{bp}$), a proxy for particles in the ~ 0.2-20 µm size range (Stramski et al., 1999, 2004; Organelli et al., 2018), can serve to detect the presence of these free-living bacteria and those associated with small-suspended particles.

Time series of $b_{bp}$ acquired by biogeochemical Argo (BGC-Argo) floats highlight the presence of a permanent layer of suspended small particles in upper suboxic ODZs ($b_{bp}$-*layer*) (Whitmire et al., 2009; Wojtasiewicz et al., 2018). It has been hypothesized that this $b_{bp}$-*layer* is linked to $N_2$-yielding microbial communities such as denitrifying and anammox bacteria. However, this hypothesis has not yet been clearly demonstrated. To address this, the first step is to evaluate: (1) potential correlations between the biogeochemical factors that control the presence of the $b_{bp}$-*layer* and denitrifying-anammox bacteria ($O_2$, $NO_3^-$, OM, $H_2S$, Murray et al., 1995; Ward et al., 2008; Dalsgaard et al., 2014; Bristow et al., 2016), and (2) the possible relationship between the $b_{bp}$-*layer* and $N_2$ produced by microbial communities.

This first step is thus essential for identifying the origin of the $b_{bp}$-*layer* and, ultimately, determining if BGC-Argo observations of $b_{bp}$ can be implemented to delineate the suboxic zone where such bacteria are confined. The Black Sea appears as a suitable area for probing into the origin of the $b_{bp}$-*layer* in suboxic waters in this way. It is indeed a semi-enclosed suboxic-anoxic basin where $N_2$ production and related denitrifying and anammox bacteria are mainly confined within a well-defined suboxic zone (Kuypers et al., 2003; Konovalov et al., 2005; Kirkpatrick et al., 2012). In addition, a permanent $b_{bp}$-*layer* is a typical characteristic of this region (Stanev et al., 2017, 2018).

The goal of our study is therefore to investigate the origin of the $b_{bp}$-*layer* in the suboxic waters of the Black Sea using data collected by BGC-Argo floats. More specifically, we aim to evaluate, within the suboxic zone, how: (1) two of the main factors ($O_2$ and $NO_3^-$) that drive the dynamics of denitrifying and anammox bacteria, impact on the location and thickness of the $b_{bp}$-*layer*, (2) $NO_3^-$ controls the vertical distribution of $b_{bp}$ within this layer, (3) temperature drives the formation of the $b_{bp}$-*layer* and consumption rates of $NO_3^-$, and (4) particle content inferred from $b_{bp}$ and $N_2$ produced by microbial communities are at least qualitatively correlated. Ultimately, our findings allow us to infer that $b_{bp}$ can potentially be used to detect the presence of the microbial communities that drive $N_2$ production in the upper suboxic waters masses – *including denitrifying-anammox bacteria*.

## 2 Methods

### 2.1 Bio-optical and physicochemical data measured by BGC-Argo floats

We used data collected by three BGC-Argo floats that profiled at a temporal resolution of 5-10 days in the first 1000 m depth of the Black Sea from December 2013 to July 2019 (Figure 1). These floats — allocated the World Meteorological Organization (WMO) numbers 6900807, 6901866, and 7900591 — collected 239, 301, and 518 vertical profiles, respectively. BGC-Argo float 6901866 was equipped with four sensors: (1) a SBE-41 CP conductivity-T-depth sensor (Sea-Bird Scientific), (2) an Aanderaa 4330 optode (serial number:1411), (3) a WETLabs ECO Triplet Puck, and (4) a Satlantic Submersible

https://doi.org/10.5194/bg-2020-167
Preprint. Discussion started: 8 June 2020


Biogeosciences Discussions Open Access EGU

Ultraviolet Nitrate Analyzer (SUNA). These sensors measured upward profiles of: (1) temperature (T), conductivity, and depth, (2) dissolved oxygen ($O_2$), (3) chlorophyll fluorescence, total optical backscattering (particles + pure seawater) at 700 nm and fluorescence by Colored Dissolved Organic Matter, and (4) nitrate ($NO_3^-$) and bisulfide ($HS^-$). Floats 6900807 and 7900591 were equipped with only the first three sensors.

Raw data of fluorescence and total backscattering were converted into Chlorophyll concentration (*chl*) and particle backscattering ($b_{bp}$) following standard protocols (Schmechtig et al., 2014, 2015). Spike signals in vertical profiles of *chl* and $b_{bp}$ ~~and~~ due to particle aggregates were removed by using a median filter with a window size of three data points (Briggs et al., 2011). $NO_3^-$, $HS^-$ and $O_2$ data were processed following BGC-Argo protocols (Johnson et al., 2018; Thierry et al., 2018). Sampling regions covered by the three floats encompassed most of the Black Sea area (Figure 1, and Appendix A). However, we only used data collected during periods without a clear injection of small particles derived from the productive layer and Bosporus plume (e.g. advection of water masses, Stanev et al., 2017). This restriction allowed us to focus on the *in-situ* 1D processes driving local formation of the $b_{bp}$-*layer*, with minimal interference from any possible external sources of small particles.

We only describe the time series of data collected by float 6901866 because this was the only float carrying a $NO_3^-$/$HS^-$ sensor. Data acquired by floats 6900807 and 7900591 are described in Appendix A, and nevertheless used as complementary data to those of float 6901866 to corroborate: (1) qualitative correlations between $O_2$ levels and the location of the $b_{bp}$-*layer*, and (2) consistency in the location of the $b_{bp}$ maximum within the $b_{bp}$-*layer*.

### 2.2 Defining the suboxic zone, mixed layer depth, and productive layer

We used $O_2$ and $NO_3^-$ to respectively define the top and bottom isopycnals of the suboxic zone where denitrifying and anammox bacteria are expected to be found. To set the top isopycnal, we applied an $O_2$ threshold of ~3 µM because denitrifying and anammox bacteria seem to tolerate $O_2$ concentrations beneath this threshold (Jensen et al., 2008; Babbin et al., 2014). The bottom isopycnal was defined as the deepest isopycnal at which $NO_3^-$ was detected by the SUNA sensor (0.23 ± 0.32 µM). $NO_3^-$ was used to set this isopycnal because heterotrophic denitrification and subsequent reactions cannot occur without $NO_3^-$ (Lam et al., 2009; Bristow et al., 2017). $HS^-$ was not used to delimit the bottom of this zone because the maximum concentration of $H_2S$ that denitrifying and anammox bacteria tolerate is not well established (Murray et al., 1995; Kirkpatrick et al., 2012; see also section 3.1).

Mixed layer depth (MLD) was computed as the depth at which density differed from 0.03 kg $m^{-3}$ with respect to the density recorded at 1m depth (de Boyer Montégut et al., 2004). We used *chl* to define the productive layer where living phytoplankton were present and producing particulate organic carbon. The base of this layer was set as the depth at which *chl* decreased below 0.25 mg $m^{-3}$. This depth was used only as a reference to highlight the periods when surface-derived small particles were clearly injected into the suboxic zone.

### 2.3 Complementary cruise data on $N_2$ excess and $NO_3^-$

Published data on $N_2$:Ar ratios and $NO_3^-$ collected at the southwest of the Black Sea in March 2005 (Fuchsman et al., 2008, 2019) were exploited to complement discussion of our results. $N_2$ produced by anaerobic microbial communities ($N_2$ excess, µM) was estimated from $N_2$:Ar ratios and argon concentrations at atmospheric saturation (Hamme and Emerson, 2004). $N_2$ excess data were used to: (1) describe the suboxic zone where $N_2$ is expected to be predominantly produced, and (2) highlight

https://doi.org/10.5194/bg-2020-167
Preprint. Discussion started: 8 June 2020


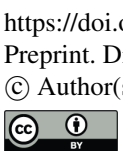

Biogeosciences Discussions Open Access EGU

qualitative correlations between $N_2$ excess, the location of the $b_{bp}$-*layer*, and vertical distribution of small particles within the $b_{bp}$-*layer*.

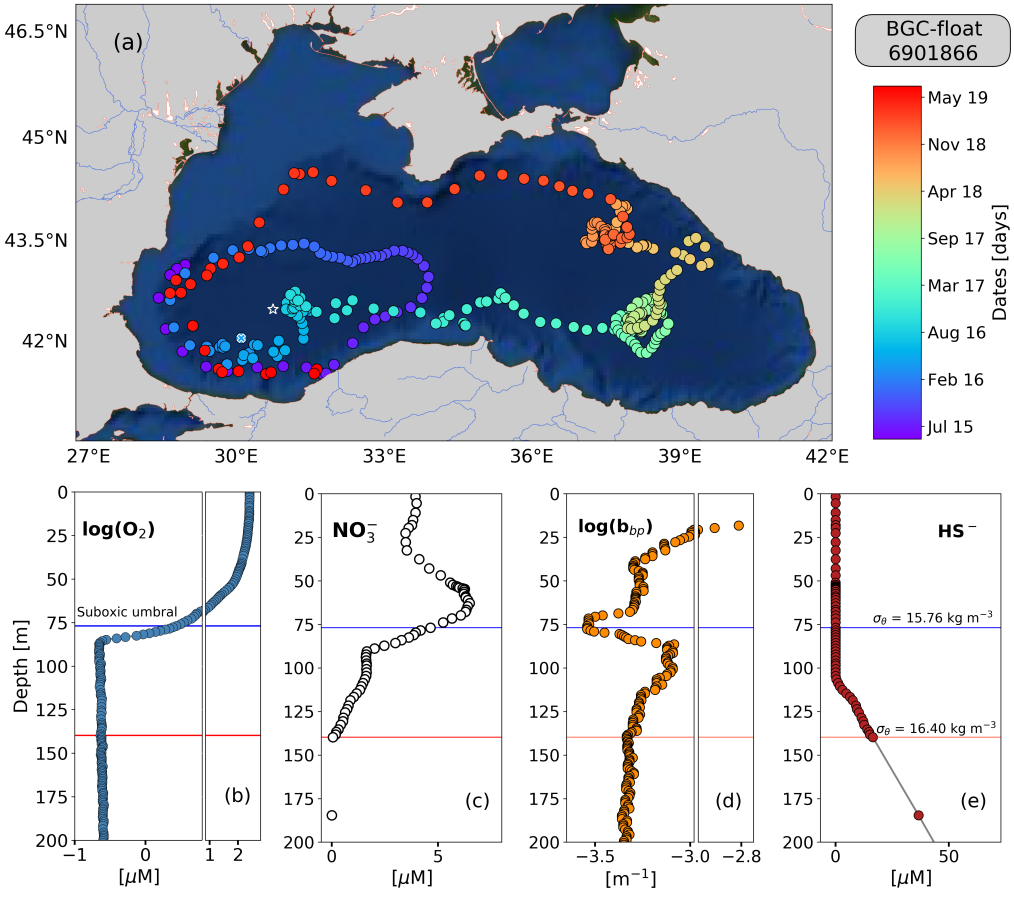


**Figure 1: (a) Sampling locations of float 6901866 between May 2015 and July 2019. Colored circles indicate the date (color bar) for a given profile. The white star in (a) marks the sampling site of the cruise (March 2005). The white *x* in (a) highlights the float location on 6th April 2016. Float profiles of (b) log($O_2$), (c) $NO_3^-$, (d) log($b_{bp}$), and (e) $HS^-$ collected on 24th November 2018.**

## 3 Results and discussion

### 3.1 Description of the suboxic zone

The top and bottom of the suboxic zone are located around the isopycnals (mean ± standard deviation) 15.79 ± 0.23 kg $m^{-3}$ and 16.30 ± 0.09 kg $m^{-3}$, respectively. The two isopycnals therefore delimit the suboxic zone where denitrifying and anammox bacteria are expected to be found (zone hereafter called $SO_{D\text{-}A}$, Figure 2). The top location and thickness of the $SO_{D\text{-}A}$ show large spatial-temporal variability, ranging between 80-180 m and 30-80 m, respectively (Figure 2). The bottom of the $SO_{D\text{-}A}$ is slightly sulfidic ($HS^-$ = 11.4 ± 3.53 µM, n = 86) and deeper than suggested (e.g. $\sigma_\theta$ = 16.20 kg $m^{-3}$, and $H_2S \leq 10$ nM, Murray

https://doi.org/10.5194/bg-2020-167
Preprint. Discussion started: 8 June 2020


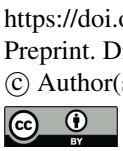

Biogeosciences Discussions Open Access EGU

et al., 1995). However, our results coincide with the slightly sulfidic conditions of the deepest isopycnal at which anammox bacteria can be still recorded ($\sigma_\theta$ = 16.30 kg m$^{-3}$, and $H_2S \geq 10$ µM, Kirkpatrick et al., 2012).

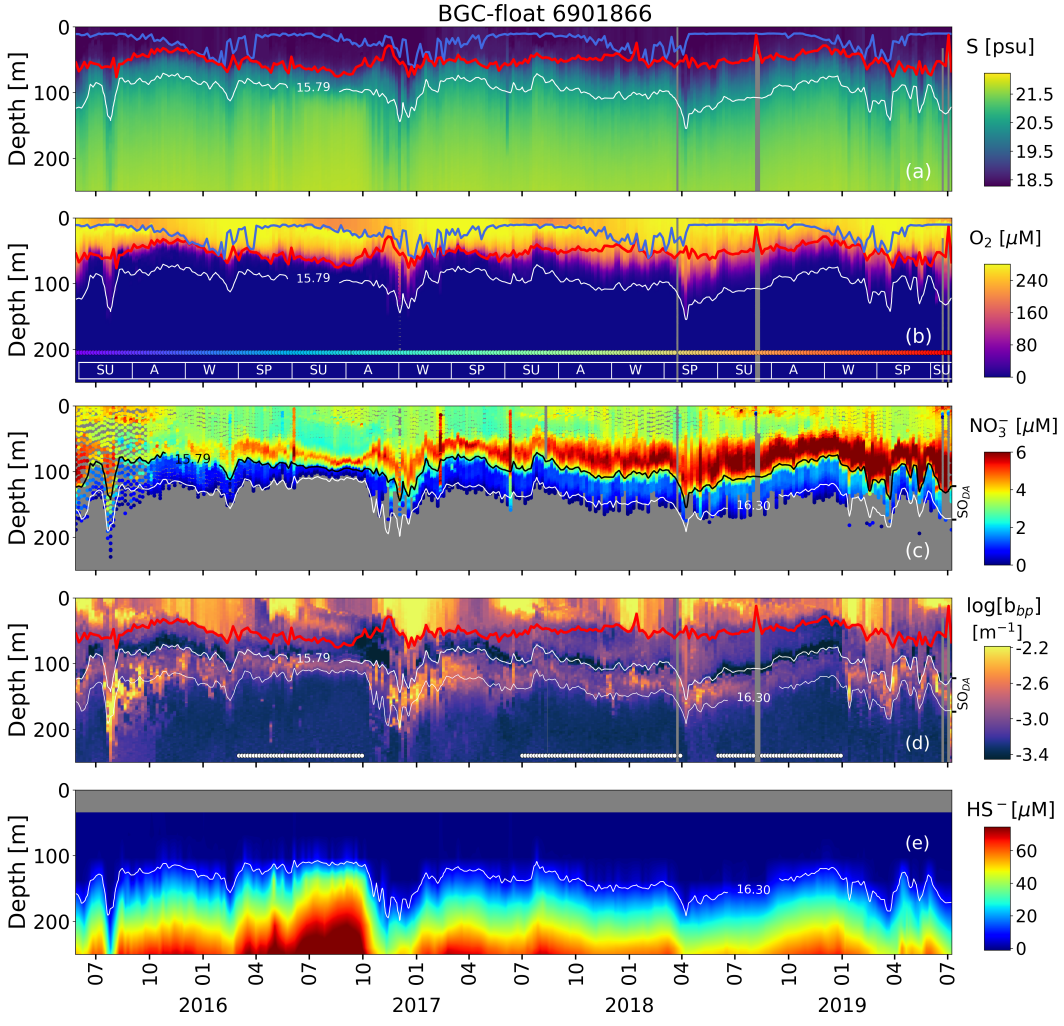


**Figure 2: Time series of: (a) Salinity (S), (b) $O_2$, (c) $NO_3^-$, (d) log($b_{bp}$), and (e) $HS^-$. The blue lines in (a) and (b) indicate the mixed layer depth. The red lines in (a), (b) and (d) show the base of the productive region. The isopycnals 15.79 kg m$^{-3}$ and 16.30 kg m$^{-3}$ describe the top and bottom of the suboxic zone ($SO_{D\text{-}A}$), respectively. SU, A, W, and SP stand for summer, autumn, winter, and spring, respectively. The colored horizontal line in (b) indicates the sampling site for a given date (Figure 1). The horizontal white lines in (d) are the profiles used to: (1) delimit the $SO_{D\text{-}A}$, and (2) compute correlations between $b_{bp}$, $NO_3^-$, and T within the $SO_{D\text{-}A}$.**

### 3.2 $NO_3^-$ and $O_2$ as key drivers of the thickness and location of the suspended small-particle layer

The permanent $b_{bp}$-*layer* is always confined within the two isopycnals that delimit the $SO_{D\text{-}A}$ (Figure 2). It follows that the thickness and top location of this layer demonstrate the same spatial and temporal variability as the one described for the $SO_{D\text{-}}$

https://doi.org/10.5194/bg-2020-167
Preprint. Discussion started: 8 June 2020


Biogeosciences Discussions Open Access EGU

135 $_A$ (Figure 2 and Appendix A). This correlation indicates that variations in the thickness and top location of the $b_{bp}$-*layer* are
136 partially driven, respectively, by: (1) the amount of $NO_3^-$ available to produce $N_2$ inside the $SO_{D\text{-}A}$, and (2) downward ventilation
137 of oxygen-rich subsurface waters (Figure 2 and Appendix A).

138 $NO_3^-$ and $O_2$ are two of the key factors that modulate the presence of denitrifying and anammox bacteria (Ulloa et al., 2012;
139 Bristow et al., 2017). Therefore, the results described above highlight that at least a fraction of the $b_{bp}$-*layer* should be due to
140 these bacteria. This notion is supported by three main observations. Firstly, the top location of the $b_{bp}$-*layer* is driven by the
141 intrusion of subsurface water masses ($S \leq 20.36 \pm 0.18$ psu) with $O_2$ concentrations above the levels tolerated by denitrifying
142 and anammox bacteria ($O_2 \geq 3$ $\mu$M, Jensen et al., 2008; Babbin et al., 2014; Figure 2). As a result, in regions where $O_2$ is
143 ventilated to deeper water masses, the top location of the $b_{bp}$-*layer* is also deeper. The contrary is observed when $O_2$ ventilation
144 is shallower (Figure 2 and Appendix A). Secondly, denitrifying and anammox bacteria reside between the isopycnals 15.60-
145 16.30 kg m$^{-3}$ (Fuchsman et al., 2012a; Kirkpatrick et al., 2012), while the $b_{bp}$-*layer* is formed between isopycnals ~15.79-16.30
146 kg m$^{-3}$. We can thus infer coexistence of such bacteria between the coincident isopycnals where the $b_{bp}$-*layer* is generated.
147 Thirdly, $NO_3^-$ declines from around isopycnal 15.79 kg m$^{-3}$ to the isopycnal 16.30 kg m$^{-3}$ due to the expected $N_2$ production
148 (Figures 2-3, and Kirkpatrick et al., 2012).

149 Overall, the qualitative evidence presented above points out that denitrifying and anammox bacteria are likely to represent at
150 least a fraction of the $b_{bp}$-*layer*. However, it is also known that these bacteria produce $N_2$ coupled with sulfur-oxidizing bacteria,
151 and generate inorganic particles as intermediaries (e.g. MnOx, Johnson, 2006; Canfield et al., 2010; Fuchsman et al., 2012b;
152 Callbeck et al., 2018; Stanev et al., 2018). Ultimately, both bacteria communities and inorganic particles appear to contribute
153 to the formation of the $b_{bp}$-*layer*. This observation leads us to argue, in the next section, that the $b_{bp}$-*layer* is partially composed
154 of $N_2$-yielding microbial communities such as *anammox and denitrifying* bacteria.

155 **3.3 Role of the removal rate of $NO_3^-$ and of temperature in the vertical distribution of small particles**

156 We propose that the removal rate of $NO_3^-$ is a key driver of the vertical distribution of small particles and $N_2$ excess within the
157 $SO_{D\text{-}A}$. This is because the vertical profiles of small particles and of $N_2$ excess are qualitatively similar, and both profiles are
158 clearly related to the rate at which $NO_3^-$ is removed from the $SO_{D\text{-}A}$ (Figures 3-4). For instance, maxima of $N_2$ excess and $b_{bp}$
159 coincide around the isopycnal 16.11 ± 0.11 kg m$^{-3}$ (Figure 3, Konovalov et al., 2005; Fuchsman et al., 2008, 2019). At this
160 isopycnal, the mean concentration of $NO_3^-$ is 1.19 ± 0.53 µM. We thus propose that this $NO_3^-$ threshold value splits the $SO_{D\text{-}A}$
161 in two sub-zones with distinctive biogeochemical conditions. Ultimately, these two different sets of conditions drive the rates
162 at which $NO_3^-$ and small particles are removed and formed within the $SO_{D\text{-}A}$, respectively (Figure 3, and explanation below).

163 The first sub-zone is thus located between the top of the $SO_{D\text{-}A}$ ($\sigma_\theta$ = 15. 79 kg m$^{-3}$) and around the isopycnal 16.11 kg m$^{-3}$.
164 Here, removal rates of $NO_3^-$ (-0.16 ± 0.10 µM m$^{-1}$, Figure 4) are likely to be boosted by: (1) high content of organic matter
165 (dissolved organic carbon = 122 ± 9 µM, Margolin et al., 2016) and $NO_3^-$ (≥ 1.19 ± 0.53 µM), and (2) $O_2$ levels staying between
166 a range that maintain the yielding of $N_2$ (0.24 ± 0.04 µM ≥ $O_2$ ≤ 2.8± 0.14 µM, n = 100, the means of the minima and maxima
167 of $O_2$, respectively, in the first sub-zone). Consequently, the formation of small particles (and related $N_2$ excess) increases from
168 the top of the $SO_{D\text{-}A}$ to around the isopycnal 16.11 kg m$^{-3}$ (Figure 3). This hypothesis is in part confirmed by significant and
169 negative power-law correlations between the suspended small-particle content and $NO_3^-$ in this sub-zone (Figure 3).

170 The second sub-zone is located between isopycnal 16.11 kg m$^{-3}$ and the bottom of the $SO_{D\text{-}A}$ ($\sigma_\theta$ = 16.30 kg m$^{-3}$, Figure 3).
171 Here, $NO_3^-$ is low (≤ 1.19 ± 0.53 µM) and $O_2$ is relatively constant (0.23 ± 0.02 µM, n= 2284, mean of $O_2$ calculated in the
172 second sub-zone for all profiles). These constant levels of $O_2$ roughly correspond to those at which anammox and heterotrophic

https://doi.org/10.5194/bg-2020-167
Preprint. Discussion started: 8 June 2020


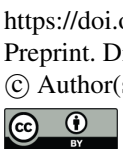

Biogeosciences Discussions
Open Access
EGU

denitrification are inhibited by ~ 50% (0.21 µM, and 0.81 µM, respectively, Dalsgaard et al., 2014). As a result, this sub-zone exhibits a decline in removal rates of $NO_3^-$ (-0.04 ± 0.01 µM $m^{-1}$, Figure 4) along with inhibited formation of small particles. Ultimately, both the content of small particles and related $N_2$ excess decrease from around isopycnal 16.11 kg $m^{-3}$ to the bottom of the $SO_{D\text{-}A}$ (Figure 3). These results are in agreement with significant and positive exponential correlations computed between the small-particle content inferred from $b_{bp}$ and $NO_3^-$ within this sub-zone (Figure 3).

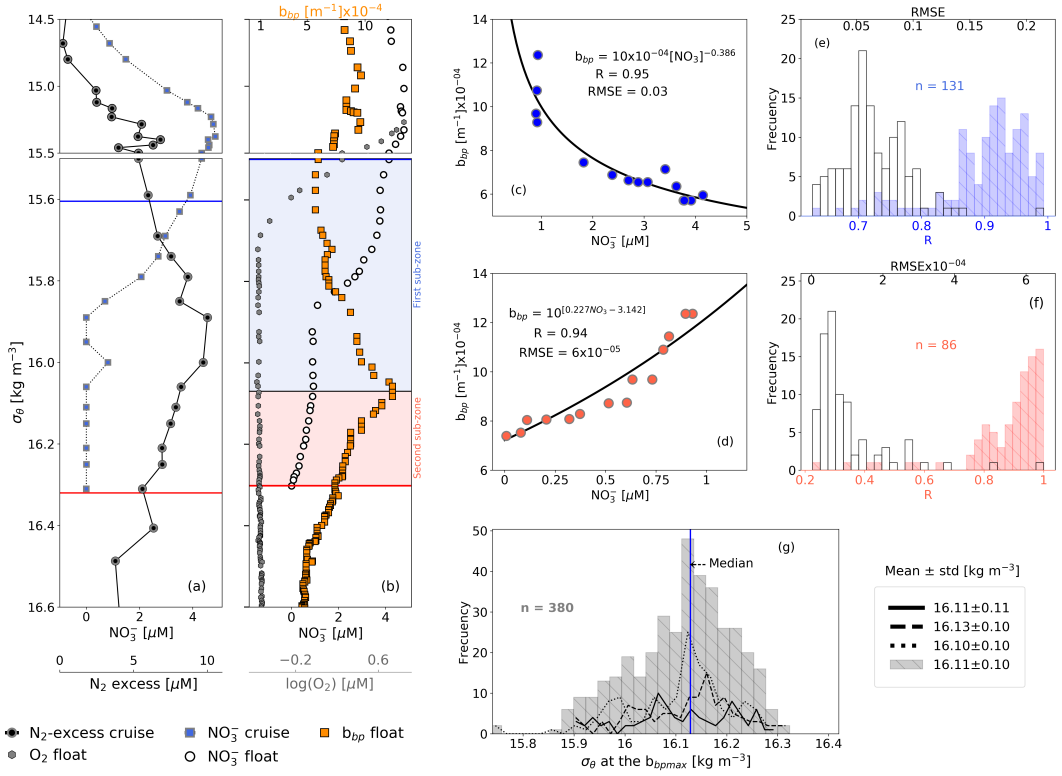


**Figure 3: (a) Cruise profiles of $NO_3^-$, and $N_2$ excess, collected in March 2005 (Fuchsman et al., 2019). (b) Float profiles of $NO_3^-$, $b_{bp}$, and log($O_2$) measured on 6th April 2016. Profiles in (a) and (b) were conducted at the northwest of the basin (see Figure 1). The top and bottom of the $SO_{D\text{-}A}$ are described in (a) and (b) as horizontal blue and red lines, respectively. The $b_{bp}$ maximum is the horizontal black line in (b). The first and second sub-zone of the $SO_{D\text{-}A}$ are respectively highlighted in (b) as blue and red squares. $NO_3^-$ vs $b_{bp}$ in (c) the first, and (d) the second sub-zone, of the float profile in (b). The number of data points visualized in (c) is lower than in (b) for the first sub-zone because $b_{bp}$ and $NO_3^-$ are not always recorded at the same depths. (e) Frequency distributions of correlation coefficients (R, blue bars), and root mean square errors (RMSE, white bars) for $NO_3^-$ vs $b_{bp}$ in the first sub-zone. (f) Same as (e) but for the second sub-zone. (g) Frequency distributions of the isopycnals at which $b_{bp}$ maxima are found within the $SO_{D\text{-}A}$. Dotted, dashed, and solid black lines in (g) are data collected by floats 7900591, 6901866, and 6900807, respectively. Gray bars include all data.**

Strong-positive linear correlations are also recorded between $b_{bp}$ and T in the first sub-zone of the $SO_{D\text{-}A}$ (Figure 4). This is likely to indicate that the formation of small particles is sensitive to very tiny increments in T (0.003 ± 0.001 °C $m^{-1}$, n = 133). We thus infer a tendency for the decline rates of $NO_3^-$ and related production of $N_2$ to increase with T. This hypothesis is at least partially supported by the significant correlation between $NO_3^-$ decline rates and T increase rates in this sub-zone (Figure

https://doi.org/10.5194/bg-2020-167
Preprint. Discussion started: 8 June 2020


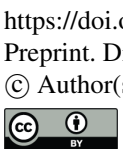

Biogeosciences Discussions
Open Access
EGU

4). Within the second sub-zone, T continues increasing while $b_{bp}$ decreases, likely due to inhibition of the formation of small particles for the reasons described above (Figure 4). These observations suggest that the production of small particles is likely to have first- and second-order covariations, with $NO_3^-$ and T, respectively — a likelihood backed up by a lack of correlation between $NO_3^-$ decline rates and T increase rates in this sub-zone (Figure 4). However, we admittedly cannot discount the possibility that the decline in $b_{bp}$ may also be due to the dissolution of MnOx just beneath the isopycnal 16.11 kg $m^{-3}$ (e.g. Konovalov et al., 2003, 2005, 2006).

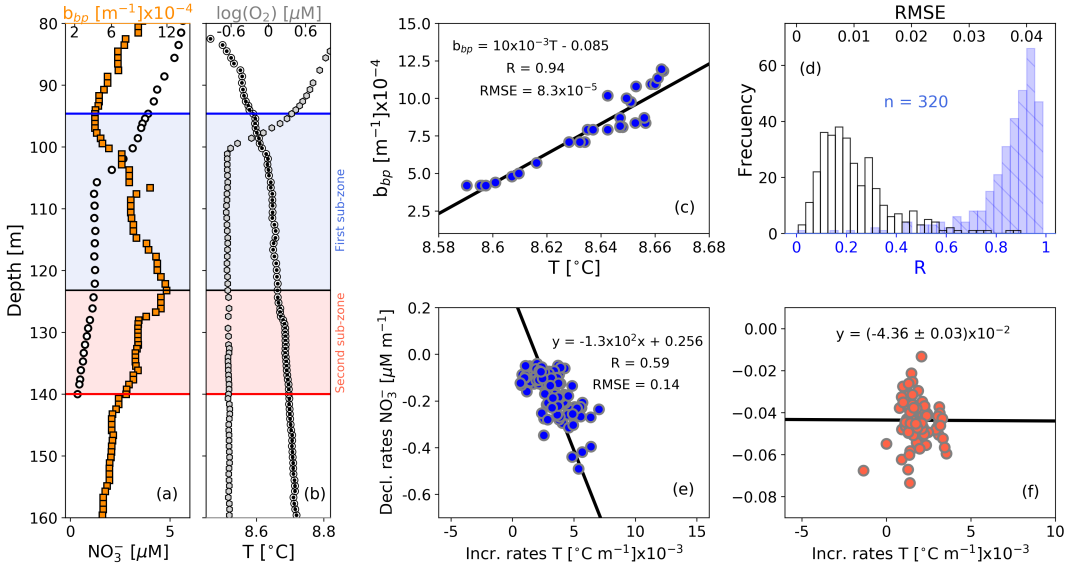


**Figure 4: Float profiles of (a) $NO_3^-$, and $b_{bp}$, and (b) T and log($O_2$) collected on 10th September 2017. Horizontal blue and red lines in (a) and (b) are the top and bottom of the $SO_{D\text{-}A}$. The $b_{bp}$ maximum is indicated in (a) and (b) as horizontal black lines. The first and second sub-zones of the $SO_{D\text{-}A}$ are respectively highlighted in (a) and (b) as blue and red squares. (c) $b_{bp}$ vs T for the first sub-zone of the profile in (b). (d) Frequency distributions of correlation coefficients (R, blue bars), and root mean square errors (RMSE, white bars), for $b_{bp}$ vs T in the first sub-zone, including data collected by the three floats. Decrease rates of $NO_3^-$ vs increase rates of T in (e) the first and (f) the second sub-zone.**

To summarize, BGC-Argo float data combined with a proxy of $N_2$ production suggest that the *$b_{bp}$-layer* is *at least partially* composed of anaerobic microbial communities involved in the production of $N_2$. It is thus inferred that this *$b_{bp}$-layer* includes *anammox and denitrifying* bacteria. These results also suggest that $N_2$ production rates can be highly variable in the Black Sea because the characteristics of the *$b_{bp}$-layer* show large spatial-temporal variations driven by changes in $NO_3^-$ and $O_2$ (Figures 2 and 4). Finally, we propose that $b_{bp}$ and $O_2$ can be exploited as a combined proxy for defining the $N_2$-producing section of the suboxic Black Sea. We consider that this combined proxy can delineate the top and base of this section, by applying an $O_2$ threshold of 3.0 µM, and the bottom isopycnal of the *$b_{bp}$-layer*, respectively. This section should thus be linked to free-living bacteria (0.2-2 µm), and those associated with small-suspended particles (> 2-20 µm).

https://doi.org/10.5194/bg-2020-167
Preprint. Discussion started: 8 June 2020




### 3.4 New perspectives for studying $N_2$ losses in suboxic ODZs

The conclusions and inferences of this study, especially those related to the origin and drivers of the $b_{bp}$-*layer*, primarily apply to the Black Sea. However, these findings may also have a wider application. In particular, suboxic ODZs are similarly characterized by the formation of a layer of suspended small particles that can be optically detected by $b_{bp}$ and the attenuation coefficients of particles (Spinrad et al., 1989; Naqvi et al., 1993; Whitmire et al., 2009). This layer is linked to $N_2$-yielding microbial communities because its location coincides with the maxima of $N_2$ excess, microbial metabolic activity, and nitrite ($NO_2^-$, the intermediate product of denitrification-anammox that is mainly accumulated in the $N_2$-yielding section, Spinrad et al., 1989; Naqvi et al., 1991, 1993; Devon et al., 2006; Chang et al., 2010, 2012; Ulloa et al., 2012; Wojtasiewicz et al., 2018). Therefore, our findings suggest that highly resolved vertical profiles of $b_{bp}$ and $O_2$ can potentially be used as a combined proxy to define the *effective* $N_2$-production section of suboxic ODZs. Such definition can be key to better-constrained global estimates of $N_2$ loss rates because it can allow us to: (1) accurately predict the suboxic water volume where around 90% of $N_2$ is produced in the ODZ core (Babin et al., 2014), and (2) evaluate how the location and thickness of the $N_2$-yielding section vary due to changes in the biogeochemical factors that modulate anammox and heterotrophy denitrification.

Global estimates of $N_2$ losses differ by 2-3 fold between studies (e.g. 50-150 Tg N $yr^{-1}$, Codispoti et al., 2001; Bianchi et al., 2012, 2018; DeVries et al., 2012; Wang et al., 2019). These discrepancies are caused in part by inaccurate estimations of the suboxic volume of the $N_2$-production section. Other sources of uncertainties arise from the methods applied to estimate the amount of POC that fuels $N_2$ production. For instance, POC fluxes and their subsequent attenuation rates are not well resolved because they are computed respectively from satellite-based primary-production algorithms and generic power-law functions (Bianchi et al., 2012, 2018; DeVries et al., 2012). POC-flux estimates based on these algorithms visibly exclude: (1) POC supplied by zooplankton migration (Kiko et al., 2017; Tutasi and Escribano, 2020), (2) substantial events of POC export decoupled from primary production (Karl et al., 2012), and (3) the role of small particles derived from the physical and biological fragmentation of larger ones (Karl et al., 1988; Briggs et al., 2020). In addition, these estimates do not take into consideration the inhibition effect that $O_2$ intrusions may have on $N_2$-yield rates (Whitmire et al., 2009; Ulloa et al., 2012; Dalsgaard et al., 2014; Peters et al., 2016).

Overall, mechanistic predictions of $N_2$ losses misrepresent the strong dynamics of the biogeochemical and physical processes that regulate them. Consequently, it is still debated whether the oceanic nitrogen cycle is in balance or not (Codispoti 2007; Gruber and Galloway 2008; DeVries et al., 2012; Jayakumar et al., 2017; Bianchi et al., 2018; Wang et al., 2019). The subsiding uncertainty points to a compelling need for alternative methods that allow accurate refinement of oceanic estimations of $N_2$ losses.

Our study supports the proposition that robotic observations of $b_{bp}$ and $O_2$ can be used to better delineate the $N_2$-yielding section at the appropriate spatial (e.g. vertical and regional) and temporal (e.g. event, seasonal, interannual) resolutions. In addition, POC fluxes can be simultaneously quantified using the same float technology (BGC-Argo, Bishop et al., 2009; Dall'Olmo and Mork 2014; Boyd et al., 2019; Estapa et al., 2019; Rasse and Dall'Olmo 2019). These robotic measurements can contribute to refining global estimates of $N_2$ losses by better constraining both the suboxic zone where $N_2$ is produced, and POC fluxes that fuel its loss. Ultimately, $O_2$ intrusions into the $N_2$-yielding section can potentially be quantified by BGC-Argo floats to assess their regulatory effect on $N_2$ losses.

https://doi.org/10.5194/bg-2020-167
Preprint. Discussion started: 8 June 2020


Biogeosciences Discussions Open Access EGU

## Conclusions

Our results suggest that the $b_{bp}$-*layer* of the suboxic Black Sea is at least partially composed of anammox and denitrifying bacteria. The location and thickness of this layer show strong spatial-temporal variability, mainly driven by the ventilation of oxygen-rich subsurface waters, and nitrate available to generate $N_2$, respectively. Such variations in the characteristics of the $b_{bp}$-*layer* highlight that $N_2$-production rates can be highly variable in the Black Sea. We therefore propose that high resolution measurements of $O_2$ and $b_{bp}$ can potentially be exploited as a combined proxy to delineate the *effective* $N_2$-yielding section of ODZs. This proposition is in part supported by evidence that the $b_{bp}$-*layer* and a majority of $N_2$-yielding microbial communities are both confined in upper suboxic ODZs. We however recommend investigation into the key biogeochemical drivers of the $b_{bp}$-*layer* for each ODZ. This information will be critical for validating the applicability of the $b_{bp}$-*layer* in assessing spatial-temporal changes in $N_2$ production.

Finally, it is evident that BGC-Argo float observations can acquire essential proxies of $N_2$ production and associated drivers at appropriate spatial and temporal resolutions. The development of observation-modeling synergies therefore holds the potential to deliver an unprecedented view of $N_2$-loss drivers if robotic observations become an integrated part of model validation. Ultimately, this approach could prove essential for reducing present uncertainties in the oceanic $N_2$ budget.

https://doi.org/10.5194/bg-2020-167
Preprint. Discussion started: 8 June 2020


Biogeosciences
Discussions
Open Access
EGU

## Appendix A: Supplementary Figures

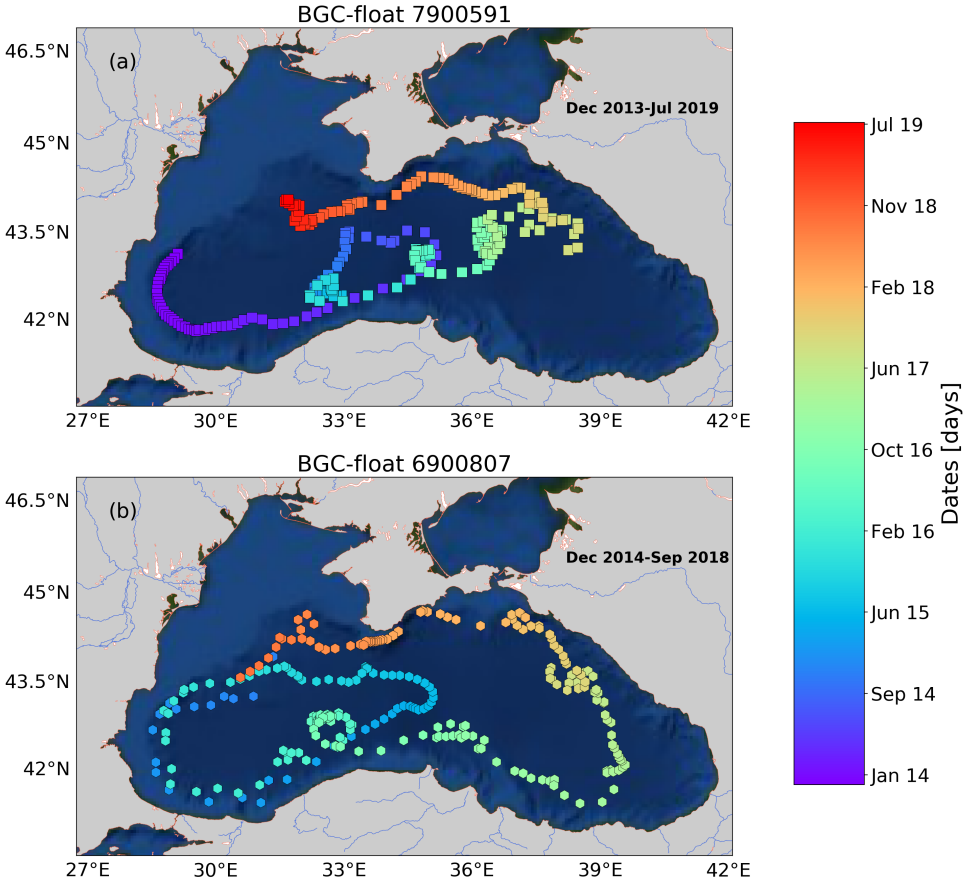


**Figure A1: Sampling locations of floats (a) 7900591 and (b) 6900807 between December 2013 and July 2019. Colored squares and hexagons indicate the date (colorbar) for a given profile of floats 6900807 and 7900591, respectively.**

https://doi.org/10.5194/bg-2020-167
Preprint. Discussion started: 8 June 2020


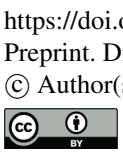

Biogeosciences Discussions Open Access EGU

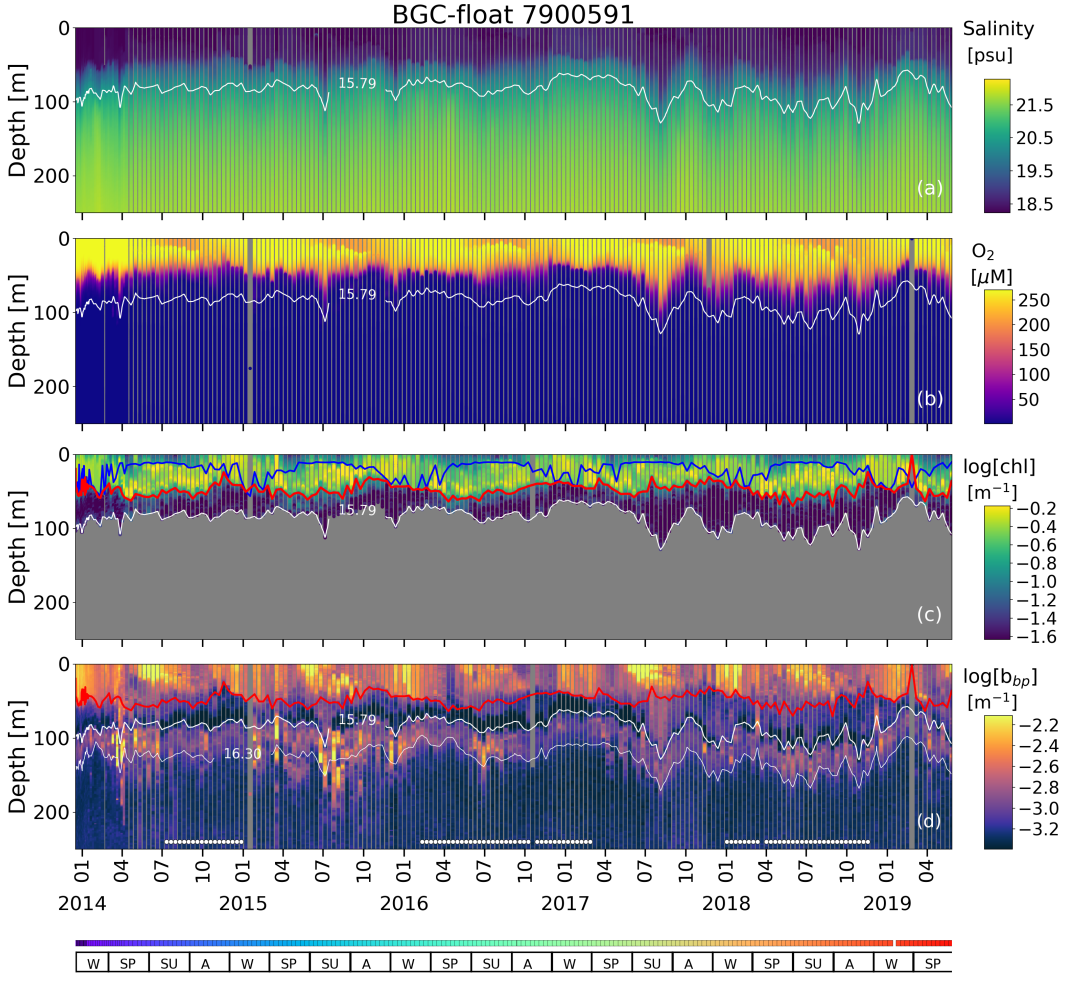


**Figure A2: Time series of (a) S, (b) $O_2$, (c) log(*chl*), and (d) log($b_{bp}$) for float 7900591. The blue line in (c) indicates the mixed layer depth. The red lines in (c) and (d) show the base of the productive region. The isopycnals 15.79 kg m$^{-3}$ and 16.30 kg m$^{-3}$ describe the top and bottom of the suboxic zone ($SO_{D\text{-}A}$), respectively. SU, A, W, and SP stand for summer, autumn, winter, and spring, respectively. The colored horizontal line at the bottom indicates the sampling site for a given date (Figure S1). The horizontal white lines in (d) are the profiles used to: (1) delimit the $SO_{D\text{-}A}$, and (2) find the isopycnals at which $b_{bp}$ is maximum in the $SO_{D\text{-}A}$. *chl* is set to zero in the $SO_{D\text{-}A}$ due to fluorescence contamination (Stanev et al., 2017).**

https://doi.org/10.5194/bg-2020-167
Preprint. Discussion started: 8 June 2020


Biogeosciences Discussions Open Access EGU

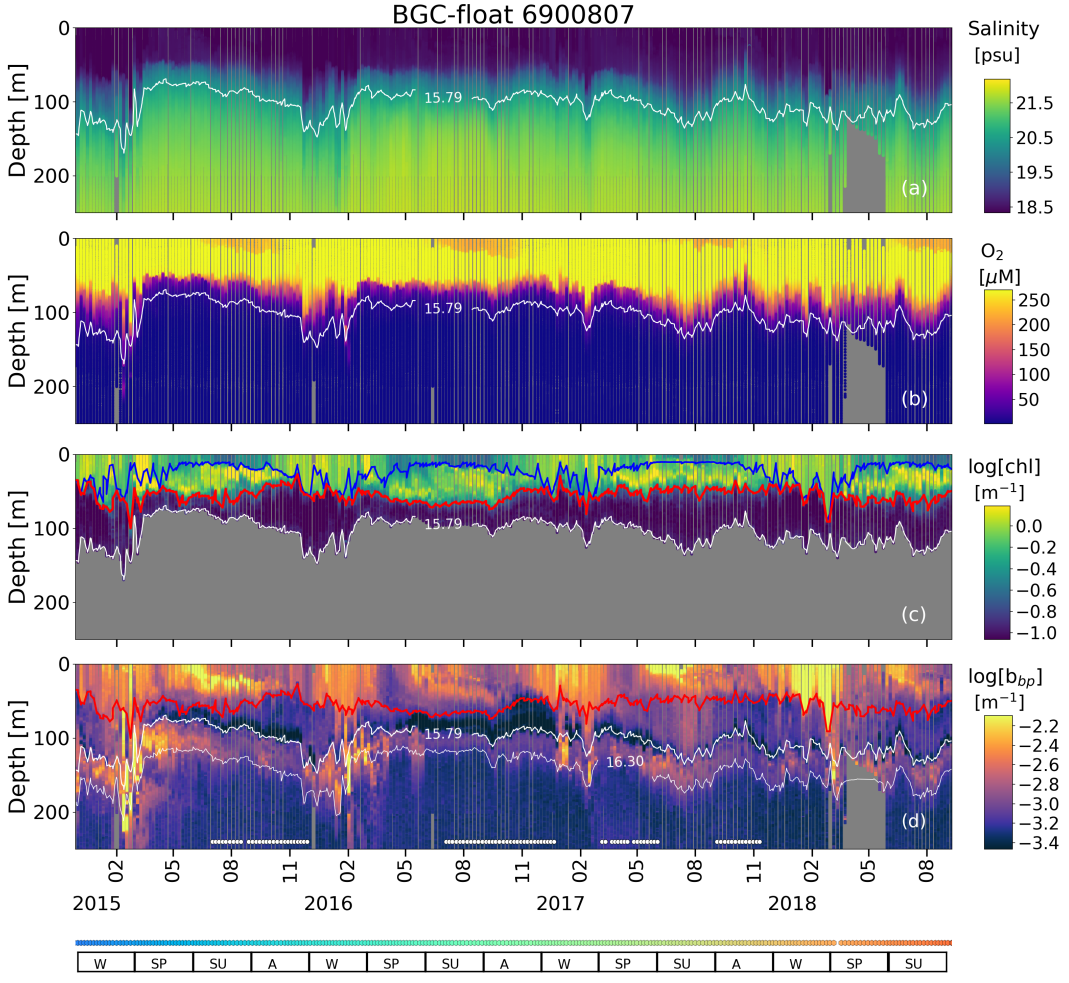


**Figure A3: Same as Figure A2 but for float 6900807**

*Data availability*. Data from Biogeochemical-Argo floats used in this study are freely available at ftp.ifremer.fr/ifremer/argo. These data were collected and made freely available by the International Argo Program and the national programs that contribute to it (http://www.argo.ucsd.edu; the Argo Program is part of the Global Ocean Observing System). Data on $N_2$:Ar ratios are freely available at https://agupubs.onlinelibrary.wiley.com/doi/abs/10.1029/2018GB006032.

*Author contributions*. R.R. conceptualized the study, wrote the original draft, and generated all figures. H.C. contributed to tuning the study's conceptualization and figures design. A.P. processed all BGC-Argo float data. R.R. and H.C. reviewed and edited the final manuscript.

*Acknowledgments*. This study was conducted in the framework of the *Noceanic* project. This project is funded by the European Union's Horizon 2020 research and innovation program under the Marie Skłodowska-Curie Individual Fellowship awarded to Rafael Rasse (grant agreement 839062). This study is a contribution to the remOcean project (European Research Council, grant agreement 246777, Hervé Claustre).

https://doi.org/10.5194/bg-2020-167
Preprint. Discussion started: 8 June 2020




*Competing interests*. The authors declare that they have no conflicts of interest.

**References**

Alldredge, A. L., and Cohen, Y.: Can microscale chemical patches persist in the sea? Microelectrode study of marine snow, fecal pellets, Science, 235(4789), 689-691, DOI: 10.1126/science.235.4789.689, 1987

Altabet, M. A., Ryabenko, E., Stramma, L., Wallace, D. W., Frank, M., Grasse, P., and Lavik, G.: An eddy-stimulated hotspot for fixed nitrogen-loss from the Peru oxygen minimum zone, Biogeosciences, 9, 4897-4908, https://doi.org/10.5194/bg-9-4897-2012, 2012

Babbin, A. R., Keil, R. G., Devol, A. H., and Ward, B. B.: Organic matter stoichiometry, flux, and oxygen control nitrogen loss in the ocean, Science, 344(6182), 406-408, DOI: 10.1126/science.1248364, 2014.

Bianchi, D., Dunne, J. P., Sarmiento, J. L., and Galbraith, E. D.: Data-based estimates of suboxia, denitrification, and $N_2O$ production in the ocean and their sensitivities to dissolved $O_2$, Global Biogeochem. Cy., 26(2), 2012.

Bianchi, D., Weber, T. S., Kiko, R., and Deutsch, C.: Global niche of marine anaerobic metabolisms expanded by particle microenvironments, Nat. Geosci., 11(4), 263-268, https://doi.org/10.1038/s41561-018-0081-0, 2018.

Bishop, J. K., and Wood, T. J.: Year-round observations of carbon biomass and flux variability in the Southern Ocean, Global Biogeochem. Cy., 23(2), https://doi.org/10.1029/2008GB003206, 2009.

Boyd, P. W., Claustre, H., Levy, M., Siegel, D. A., and Weber, T.: Multi-faceted particle pumps drive carbon sequestration in the ocean, Nature, 568(7752), 327-335, https://doi.org/10.1038/s41586-019-1098-2, 2019.

Briggs, N., Perry, M. J., Cetinić, I., Lee, C., D'Asaro, E., Gray, A. M., and Rehm, E.: High-resolution observations of aggregate flux during a sub-polar North Atlantic spring bloom, Deep-Sea Res. Pt. I., 58(10), 1031–1039, https://doi.org/10.1016/j.dsr.2011.07.007, 2011.

Briggs, N., Dall'Olmo, G., and Claustre, H.: Major role of particle fragmentation in regulating biological sequestration of $CO_2$ by the oceans, Science, 367(6479), 791-793, DOI: 10.1126/science.aay1790, 2020.

Bristow, L.A., Dalsgaard, T., Tiano, L., Mills, D.B., Bertagnolli, A.D., Wright, J.J., Hallam, S.J., Ulloa, O., Canfield, D.E., Revsbech, N.P. and Thamdrup, B. : Ammonium and nitrite oxidation at nanomolar oxygen concentrations in oxygen minimum zone waters, Proc. Natl. Acad. Sci. U. S. A., 113(38), 10601-10606, https://doi.org/10.1073/pnas.1600359113, 2016.

Bristow, L.A., Callbeck, C.M., Larsen, M., Altabet, M.A., Dekaezemacker, J., Forth, M., Gauns, M., Glud, R.N., Kuypers, M.M., Lavik, G. and Milucka, J.: $N_2$ production rates limited by nitrite availability in the Bay of Bengal oxygen minimum zone, Nat. Geosci., 10(1), 24-29, https://doi.org/10.1038/ngeo2847, 2017.

Chang, B. X., Devol, A. H., and Emerson, S. R.: Denitrification and the nitrogen gas excess in the eastern tropical South Pacific oxygen deficient zone, Deep-Sea Res. Pt. I., 57(9), 1092-1101, https://doi.org/10.1016/j.dsr.2010.05.009, 2010.

https://doi.org/10.5194/bg-2020-167
Preprint. Discussion started: 8 June 2020




Chang, B. X., Devol, A. H., and Emerson, S. R.: Fixed nitrogen loss from the eastern tropical North Pacific and Arabian Sea oxygen deficient zones determined from measurements of $N_2$:Ar, Global Biogeochem. Cy., 26(3), https://doi.org/10.1029/2011GB004207, 2012.

Callbeck, C.M., Lavik, G., Ferdelman, T.G., Fuchs, B., Gruber-Vodicka, H.R., Hach, P.F., Littmann, S., Schoffelen, N.J., Kalvelage, T., Thomsen, S. and Schunck, H.: Oxygen minimum zone cryptic sulfur cycling sustained by offshore transport of key sulfur oxidizing bacteria, Nat. Commun., 9(1), 1-11, https://doi.org/10.1038/s41467-018-04041-x, 2018.

Canfield, D.E., Stewart, F.J., Thamdrup, B., De Brabandere, L., Dalsgaard, T., Delong, E.F., Revsbech, N.P. and Ulloa, O.: A cryptic sulfur cycle in oxygen-minimum–zone waters off the Chilean coast, Science, 330(6009), 1375-1378, DOI: 10.1126/science.1196889, 2010.

Codispoti, L. A.: An oceanic fixed nitrogen sink exceeding 400 Tg N $a^{-1}$ vs the concept of homeostasis in the fixed-nitrogen inventory, Biogeosciences, 4, 233–253, https://doi.org/10.5194/bg-4-233-2007, 2007.

Codispoti, L. A., Brandes, J. A., Christensen, J. P., Devol, A. H., Naqvi, S. W. A., Paerl, H. W., and Yoshinari, T.: The oceanic fixed nitrogen and nitrous oxide budgets: Moving targets as we enter the anthropocene?, Sci. Mar., 65(S2), 85-105, 2007.

Dall'Olmo, G., and Mork, K. A.: Carbon export by small particles in the Norwegian Sea, Geophys. Res. Lett., 41, 2921–2927, https://doi.org/10.1002/2014GL059244, 2014.

Dalsgaard, T., Stewart, F.J., Thamdrup, B., De Brabandere, L., Revsbech, N.P., Ulloa, O., Canfield, D.E. and DeLong, E.F.: Oxygen at nanomolar levels reversibly suppresses process rates and gene expression in anammox and denitrification in the oxygen minimum zone off northern Chile, MBio., 5(6), e01966-14, 10.1128/mBio.01966-14, 2014.

Dalsgaard, T., Thamdrup, B., Farías, L., and Revsbech, N. P.: Anammox and denitrification in the oxygen minimum zone of the eastern South Pacific, Limnol. Oceanogr., 57(5), 1331-1346, https://doi.org/10.4319/lo.2012.57.5.1331, 2012.

de Boyer Montégut, C., Madec, G., Fischer, A. S., Lazar, A., and Iudicone, D.: Mixed layer depth over the global ocean: An examination of profile data and a profile-based climatology, J. Geophys. Res. Oceans, 109(C12), https://doi.org/10.1029/2004JC002378, 2004.

DeVries, T., Deutsch, C., Primeau, F., Chang, B., and Devol, A.: Global rates of water-column denitrification derived from nitrogen gas measurements, Nat. Geosci., 5(8), 547-550, https://doi.org/10.1038/ngeo1515, 2012.

Estapa, M. L., Feen, M. L., and Breves, E.: Direct observations of biological carbon export from profiling floats in the subtropical North Atlantic, Global Biogeochem. Cy., 33(3), 282-300, https://doi.org/10.1029/2018GB006098, 2019.

Fuchsman, C. A., Devol, A. H., Saunders, J. K., McKay, C., and Rocap, G.: Niche partitioning of the N cycling microbial community of an offshore oxygen deficient zone, Front. Microbiol., 8, 2384, https://doi.org/10.3389/fmicb.2017.02384, 2017.

Fuchsman, C. A., Murray, J. W., and Konovalov, S. K.: Concentration and natural stable isotope profiles of nitrogen species in the Black Sea, Mar. Chem., 111(1-2), 90-105, https://doi.org/10.1016/j.marchem.2008.04.009, 2008.

Fuchsman, C. A., Murray, J. W., and Staley, J. T.: Stimulation of autotrophic denitrification by intrusions of the Bosporus Plume into the anoxic Black Sea, Front. Microbiol., 3, 257, https://doi.org/10.3389/fmicb.2012.00257, 2012b.

https://doi.org/10.5194/bg-2020-167
Preprint. Discussion started: 8 June 2020




352 Fuchsman, C. A., Paul, B., Staley, J. T., Yakushev, E. V., and Murray, J. W.: Detection of transient denitrification during a
353 high organic matter event in the Black Sea, Global Biogeochem. Cy., 33(2), 143-162, https://doi.org/10.1029/2018GB006032,
354 2019.

355 Fuchsman, C. A., Staley, J. T., Oakley, B. B., Kirkpatrick, J. B., and Murray, J. W.: Free-living and aggregate-associated
356 Planctomycetes in the Black Sea, FEMS Microbiol. Ecol., 80(2), 402-416, https://doi.org/10.1111/j.1574-6941.2012.01306.x,
357 2012a.

358 Ganesh, S., Bristow, L. A., Larsen, M., Sarode, N., Thamdrup, B., and Stewart, F. J.: Size-fraction partitioning of community
359 gene transcription and nitrogen metabolism in a marine oxygen minimum zone, ISME J., 9(12), 2682,
360 https://doi.org/10.1038/ismej.2015.44, 2015.

361 Ganesh, S., Parris, D. J., DeLong, E. F., and Stewart, F. J.: Metagenomic analysis of size-fractionated picoplankton in a marine
362 oxygen minimum zone, ISME J., 8(1), 187, https://doi.org/10.1038/ismej.2013.144, 2014.

363 Gaye, B., Nagel, B., Dähnke, K., Rixen, T., and Emeis, K. C.: Evidence of parallel denitrification and nitrite oxidation in the
364 ODZ of the Arabian Sea from paired stable isotopes of nitrate and nitrite, Global Biogeochem. Cy., 27(4), 1059-1071,
365 https://doi.org/10.1002/2011GB004115, 2013.

366 Gruber, N., and Sarmiento, J. L.: Global patterns of marine nitrogen fixation and denitrification, Global Biogeochem. Cy.,
367 11(2), 235-266, https://doi.org/10.1029/97GB00077, 1997.

368 Gruber, N., and Galloway, J. N.: An Earth-system perspective of the global nitrogen cycle, Nature, 451(7176), 293-296,
369 https://doi.org/10.1038/nature06592, 2008.

370 Hamme, R. C., and Emerson, S. R.: The solubility of neon, nitrogen and argon in distilled water and seawater, Deep-Sea Res.
371 Pt. I., 51(11), 1517–1528, https://doi.org/10.1016/j.dsr.2004.06.009, 2004.

372 Helm, K. P., Bindoff, N. L., and Church, J. A.: Observed decreases in oxygen content of the global ocean, Geophys. Res. Lett.,
373 38(23), https://doi.org/10.1029/2011GL049513, 2011.

374 Jayakumar, A., Chang, B. X., Widner, B., Bernhardt, P., Mulholland, M. R., and Ward, B. B.: Biological nitrogen fixation in
375 the oxygen-minimum region of the eastern tropical North Pacific ocean, ISME J., 11(10), 2356-2367,
376 https://doi.org/10.1038/ismej.2017.97, 2017.

377 Jensen, M. M., Kuypers, M. M., Gaute, L., and Thamdrup, B.: Rates and regulation of anaerobic ammonium oxidation and
378 denitrification in the Black Sea, Limnol. Oceanogr., 53(1), 23-36, https://doi.org/10.4319/lo.2008.53.1.0023, 2008.

379 Johnson, K. S.: Manganese redox chemistry revisited. Science, 313(5795), 1896-1897, DOI: 10.1126/science.1133496, 2006.

380 Johnson, K. S., Pasqueron de Fommervault, O., Serra, R., D'Ortenzio, F., Schmechtig, C., Claustre, H., and Poteau, A.:
381 Processing Bio-Argo nitrate concentration at the DAC level, doi:10.13155/46121, 2018.

382 Karl, D. M., Church, M. J., Dore, J. E., Letelier, R. M., and Mahaffey, C.: Predictable and efficient carbon sequestration in the
383 North Pacific Ocean supported by symbiotic nitrogen fixation, Proc. Natl. Acad. Sci. U. S. A., 109(6), 1842–1849,
384 https://doi.org/10.1073/pnas.1120312109, 2012.

https://doi.org/10.5194/bg-2020-167
Preprint. Discussion started: 8 June 2020




385 Karl, D. M., Knauer, G. A., and Martin, J. H.: Downward flux of particulate organic matter in the ocean: a particle
386 decomposition paradox, Nature, 332(6163), 438-441, https://doi.org/10.1038/332438a0, 1988.

387 Karstensen, J., Stramma, L., and Visbeck, M.: Oxygen minimum zones in the eastern tropical Atlantic and Pacific oceans,
388 Prog. Oceanogr., 77(4), 331-350, https://doi.org/10.1016/j.pocean.2007.05.009, 2008.

389 Keeling, R. F., and Garcia, H. E.: The change in oceanic $O_2$ inventory associated with recent global warming, Proc. Natl. Acad.
390 Sci. U. S. A., 99(12), 7848-7853, https://doi.org/10.1073/pnas.122154899, 2002.

391 Kiko, R., Biastoch, A., Brandt, P., Cravatte, S., Hauss, H., Hummels, R., Kriest, I., Marin, F., McDonnell, A.M.P., Oschlies,
392 A. and Picheral, M.: Biological and physical influences on marine snowfall at the equator, Nat. Geosci., 10(11), 852-858,
393 https://doi.org/10.1038/ngeo3042, 2017.

394 Kirkpatrick, J. B., Fuchsman, C. A., Yakushev, E., Staley, J. T., and Murray, J. W.: Concurrent activity of anammox and
395 denitrifying bacteria in the Black Sea, Front. Microbiol., 3, 256, https://doi.org/10.3389/fmicb.2012.00256, 2012.

396 Konovalov, S.K., Luther, G.I.W., Friederich, G.E., Nuzzio, D.B., Tebo, B.M., Murray, J.W., Oguz, T., Glazer, B., Trouwborst,
397 R.E., Clement, B. and Murray, K.J.: Lateral injection of oxygen with the Bosporus plume—fingers of oxidizing potential in
398 the Black Sea, Limnol. Oceanogr., 48(6), 2369-2376, https://doi.org/10.4319/lo.2003.48.6.2369, 2003.

399 Konovalov, S. K., Murray, J. W., and Luther III, g. W.: Black Sea Biogeochemistry, Oceanography, 18(2), 24,
400 https://doi.org/10.5670/oceanog.2005.39, 2005.

401 Konovalov, S. K., Murray, J. W., Luther, G. W., and Tebo, B. M.: Processes controlling the redox budget for the oxic/anoxic
402 water column of the Black Sea, Deep-Sea Res. Pt. II., 53(17-19), 1817-1841, https://doi.org/10.1016/j.dsr2.2006.03.013, 2006.

403 Kuypers, M.M., Sliekers, A.O., Lavik, G., Schmid, M., Jørgensen, B.B., Kuenen, J.G., Damsté, J.S.S., Strous, M. and Jetten,
404 M.S.: Anaerobic ammonium oxidation by anammox bacteria in the Black Sea, Nature, 422(6932), 608,
405 https://doi.org/10.1038/nature01472, 2003.

406 Lam, P., Lavik, G., Jensen, M.M., van de Vossenberg, J., Schmid, M., Woebken, D., Gutiérrez, D., Amann, R., Jetten, M.S.
407 and Kuypers, M.M.: Revising the nitrogen cycle in the Peruvian oxygen minimum zone, Proc. Natl. Acad. Sci. U. S. A.,
408 106(12), 4752-4757, https://doi.org/10.1073/pnas.0812444106, 2009.

409 Margolin, A. R., Gerringa, L. J., Hansell, D. A., and Rijkenberg, M. J.: Net removal of dissolved organic carbon in the anoxic
410 waters of the Black Sea, Mar. Chem., 183, 13-24, https://doi.org/10.1016/j.marchem.2016.05.003, 2016.

411 Murray, J. W., Codispoti, L. A., and Friederich, G. E.: Oxidation-reduction environments: The suboxic zone in the Black Sea,
412 In C. P. Huang, C. R. O'Melia, and J. J. Morgan (Eds.), Aquatic chemistry: Interfacial and interspecies processes, ACS
413 Advances in Chemistry Series (Vol. 224, pp. 157–176), Washington DC: American Chemical Society, 1995.

414 Naqvi, S.W.A.: Geographical extent of denitrification in the Arabian Sea, Oceanol. Acta, 14(3), 281-290, 1991

415 Naqvi, S. W. A., Kumar, M. D., Narvekar, P. V., De Sousa, S. N., George, M. D., and D'silva, C.: An intermediate nepheloid
416 layer associated with high microbial metabolic rates and denitrification in the northwest Indian Ocean, J. Geophys. Res.
417 Oceans, 98(C9), 16469-16479, https://doi.org/10.1029/93JC00973, 1993.

https://doi.org/10.5194/bg-2020-167
Preprint. Discussion started: 8 June 2020




418 Organelli, E., Dall'Olmo, G., Brewin, R. J., Tarran, G. A., Boss, E., and Bricaud, A.: The open-ocean missing backscattering
419 is in the structural complexity of particles, Nat. Commun., 9(1), 1–11. https://doi.org/10.1038/s41467-018-07814-6, 2018.

420 Oschlies, A., Brandt, P., Stramma, L., and Schmidtko, S.: Drivers and mechanisms of ocean deoxygenation, Nat. Geosci.,
421 11(7), 467-473, https://doi.org/10.1038/s41561-018-0152-2, 2018.

422 Peters, B. D., Babbin, A. R., Lettmann, K. A., Mordy, C. W., Ulloa, O., Ward, B. B., and Casciotti, K. L.: Vertical modeling
423 of the nitrogen cycle in the eastern tropical South Pacific oxygen deficient zone using high-resolution concentration and isotope
424 measurements, Global Biogeochem. Cy., 30(11), 1661-1681, https://doi.org/10.1002/2016GB005415, 2016.

425 Rasse, R., and Dall'Olmo, G.: Do oceanic hypoxic regions act as barriers for sinking particles? A case study in the eastern
426 tropical north Atlantic, Global Biogeochem. Cy., https://doi.org/10.1029/2019GB006305, 2019.

427 Schmechtig, C., Claustre, H., Poteau, A., and D'Ortenzio, F.: Bio-Argo quality control manual for the chlorophyll-a
428 concentration, (pp.1–13), Argo Data Management. https://doi.org/10.13155/35385, 2014.

429 Schmechtig, C., Poteau, A., Claustre, H., D'ortenzio, F., Giorgio Dall'Olmo, G., and Boss E.: Processing BGC-Argo particle
430 backscattering at the DAC level, https://doi.org/10.13155/39459, 2015.

431 Schmidtko, S., Stramma, L., and Visbeck, M. Decline in global oceanic oxygen content during the past five decades. Nature,
432 542(7641), 335–339, https://doi.org/10.1038/nature21399, 2017.

433 Spinrad, R. W., Glover, H., Ward, B. B., Codispoti, L. A., and Kullenberg, G.: Suspended particle and bacterial maxima in
434 Peruvian coastal waters during a cold water anomaly, Deep-Sea Res. Pt. I., 36(5), 715-733, 1989.

435 Stanev, E. V., Grayek, S., Claustre, H., Schmechtig, C., and Poteau, A.: Water intrusions and particle signatures in the Black
436 Sea: a Biogeochemical-Argo float investigation, Ocean Dyn., 67(9), 1119-1136, https://doi.org/10.1007/s10236-017-1077-9,
437 2017.

438 Stanev, E. V., Poulain, P. M., Grayek, S., Johnson, K. S., Claustre, H., and Murray, J. W.: Understanding the Dynamics of the
439 Oxic-Anoxic Interface in the Black Sea, Geophys. Res. Lett., 45(2), 864-871, https://doi.org/10.1002/2017GL076206, 2018.

440 Stramma, L., Johnson, G. C., Sprintall, J., and Mohrholz, V.: Expanding oxygen-minimum zones in the tropical oceans.
441 Science, 320(5876), 655–658, https://doi.org/10.1126/science.1153847, 2008.

442 Stramski, D., Boss, E., Bogucki, D., and Voss, K. J.: The role of seawater constituents in light backscattering in the ocean.
443 Prog. Oceanogr., 61(1), 27–56, https://doi.org/10.1016/j.pocean.2004.07.001, 2004.

444 Stramski, D., Reynolds, R. A., Kahru, M., and Mitchell, B. G.: Estimation of particulate organic carbon in the ocean from
445 satellite remote sensing, Science, 285(5425), 239-242, DOI: 10.1126/science.285.5425.239, 1999.

446 Thierry, V., Bittig, H., and Argo BGC Team.: Argo quality control manual for dissolved oxygen concentration. Version 2.0,
447 23 October 2018. 10.13155/46542, 2018.

448 Tutasi, P., and Escribano, R.: Zooplankton diel vertical migration and downward C into the Oxygen Minimum Zone in the
449 highly productive upwelling region off Northern Chile, Biogeosciences, 17, 455–473, https://doi.org/10.5194/bg-17-455-
450 2020, 2020.

https://doi.org/10.5194/bg-2020-167
Preprint. Discussion started: 8 June 2020




451 Ulloa, O., Canfield, D. E., DeLong, E. F., Letelier, R. M., and Stewart, F. J.: Microbial oceanography of anoxic oxygen
452 minimum zones, Proc. Natl. Acad. Sci. U. S. A., 109(40), 15996-16003, https://doi.org/10.1073/pnas.1205009109, 2012.

453 Wang, W. L., Moore, J. K., Martiny, A. C., and Primeau, F. W.: Convergent estimates of marine nitrogen fixation, Nature,
454 566(7743), 205-211, https://doi.org/10.1038/s41586-019-0911-2, 2019.

455 Ward, B. B. How nitrogen is lost, Science, 341(6144), 352-353, DOI: 10.1126/science.1240314, 2013.

456 Ward, B.B., Devol, A.H., Rich, J.J., Chang, B.X., Bulow, S.E., Naik, H., Pratihary, A. and Jayakumar, A.: Denitrification as
457 the dominant nitrogen loss process in the Arabian Sea, Nature, 461(7260), 78-81, 2009.

458 Ward, B. B., Tuit, C. B., Jayakumar, A., Rich, J. J., Moffett, J., and Naqvi, S. W. A.: Organic carbon, and not copper, controls
459 denitrification in oxygen minimum zones of the ocean, Deep-Sea Res. Pt. I., 55(12), 1672-1683,
460 https://doi.org/10.1016/j.dsr.2008.07.005, 2008.

461 Whitmire, A. L., Letelier, R. M., Villagrán, V., and Ulloa, O.: Autonomous observations of in vivo fluorescence and particle
462 backscattering in an oceanic oxygen minimum zone, Opt. Express, 17(24), 21, 992–22,004.
463 https://doi.org/10.1364/OE.17.021992, 2009.

464 Wojtasiewicz, B., Trull, T. W., Bhaskar, T. U., Gauns, M., Prakash, S., Ravichandran, M., and Hardman-Mountford, N. J.:
465 Autonomous profiling float observations reveal the dynamics of deep biomass distributions in the denitrifying oxygen
466 minimum zone of the Arabian Sea, J. Mar. Syst., https://doi.org/10.1016/j.jmarsys.2018.07.002, 2018.